

Geochemistry, Geophysics, Geosystems

RESEARCH ARTICLE

10.1029/2018GC008117

Key Points:

- Geochemical processes behind water anomalies prior to the 2016 earthquakes in Italy are investigated by chemical models
- Increased concentrations of As and V, a slight B increase, and a concomitant lowering of B isotope ratio occurred due to mineral desorption
- Desorption was triggered by an excess of deep CO₂ in groundwater, which occurred prior to the mainshock due to preseismic crustal dilation

Supporting Information:

- Supporting Information S1
- Table S1
- Data Set S1

Correspondence to:

A. Billi,
andrea.billi@cnr.it

Citation:

Boschetti, T., Barbieri, M., Barberio, M. D., Billi, A., Franchini, S., & Petitta, M. (2019). CO₂ inflow and elements desorption prior to a seismic sequence, Amatrice-Norcia 2016, Italy. *Geochemistry, Geophysics, Geosystems*, 20, 2303–2317. <https://doi.org/10.1029/2018GC008117>





Received 3 DEC 2018

Accepted 1 APR 2019

Accepted article online 9 APR 2019

Published online 16 MAY 2019

CO₂ Inflow and Elements Desorption Prior to a Seismic Sequence, Amatrice-Norcia 2016, Italy

T. Boschetti¹ , M. Barbieri² , M. D. Barberio², A. Billi³ , S. Franchini², and M. Petitta² 

¹Dipartimento di Scienze Chimiche, della Vita e della Sostenibilità Ambientale, University of Parma, Parma, Italy,

²Dipartimento di Scienze della Terra, Sapienza University of Rome, Rome, Italy, ³Consiglio Nazionale delle Ricerche, IGAG, Rome, Italy

Abstract The 2016 Mw ≥ 6.0 Amatrice-Norcia earthquakes (central Apennines, Italy) and the related seismic sequence were associated with increases in arsenic and vanadium concentrations recorded in groundwater springs a few months before the earthquakes occurred. To evaluate these signals as reliable seismic precursors and effective predictive tools, we studied the geochemical processes that caused these anomalies. Using chemical and isotope models, we show that increased concentrations of arsenic and vanadium, a slight increase in boron concentrations, and a concomitant lowering of the boron isotope ratio may be due to mineral desorption (e.g., from iron oxides and/or clays). We argue that a displacing effect on the trace elements sorbed on minerals was triggered by an excess of deep CO₂ in groundwater, which occurred prior to the main seismic event as a result of preseismic crustal dilation. Our observations confirm the pivotal role of CO₂ in the release of trace elements by alteration of solid phases and provide a new understanding of earthquake-related water chemical anomalies.

1. Introduction

Natural disasters have a great socioeconomic impact. In the last decades, studies of earthquake precursors have shown that geophysical and geochemical changes may occur prior to earthquakes of magnitude greater than 5 (Ingebritsen & Manga, 2014). Although many observed seismic precursors are related to the stress buildup before an earthquake and its following release, the effect on the different geochemical parameters and their amounts may vary depending on many factors (e.g., geodynamics, tectonics, rocks and minerals composition, and hydrology). As a result, it is very difficult to relate the geochemical anomalies to a specific process and prove that are really associated with earthquakes. Despite this, water chemical anomalies are increasingly recorded at distances between 20 km and more than 200 km from strong earthquake epicenters (Andr n et al., 2016; Chen et al., 2015; Claesson et al., 2004; De Luca et al., 2018; Grant et al., 2011; Huang et al., 2012; Igarashi et al., 1995; Inan et al., 2012; Ingebritsen & Manga, 2014; Sano & Wakita, 2016; Skelton et al., 2008, 2014, 2019; Wakita et al., 1988; Wang & Manga, 2010; W steby et al., 2014; Zeng et al., 2015).

The 2016 Amatrice and Norcia mainshocks (24 August and 30 October, respectively; Figure 1b; Chiaraluca et al., 2017; Falcucci et al., 2018) involved significant pore pressure changes and fluid movement, both at deep and shallow crustal levels (De Luca et al., 2018; Petitta et al., 2018; Tung & Masterlark, 2018), which were preceded by hydrogeochemical anomalies recorded since April 2016 in the springs of the central Apennines (Barberio et al., 2017; De Luca et al., 2018). Increases in the concentrations of arsenic and vanadium were recorded in groundwater issuing from springs monitored in the Sulmona area (S1 to S7 in Figure 1b), roughly 70 km to the southeast of the epicentral area and in a spring within the epicentral area (S8 in Figure 1b; Barberio et al., 2017). S1 to S4 are fed by deep groundwater flow, while S5–S7 are fed by local aquifers.

A preseismic and coseismic elemental contribution from bituminous-asphaltic and/or hydrothermal fluids was hypothesized (Barberio et al., 2017). However, neither additional trace elements (e.g., Ba, Ni, and Mn) nor salinity and oxygen-hydrogen stable isotope ratio changes—which should be a consequence of hydrocarbon decomposition (Bolliger et al., 1999; Tissot & Welte, 1984) and fluid mixing, respectively—were detected (Barberio et al., 2017). The possible cause of the anomalies must explain the steady characteristics of groundwater flow and the simultaneous increase of selected trace elements.

Below, partly based on previous data (Barberio et al., 2017), we explain the geochemical processes that led to the increase in As and V concentrations in groundwater, providing a new perspective on the possible link

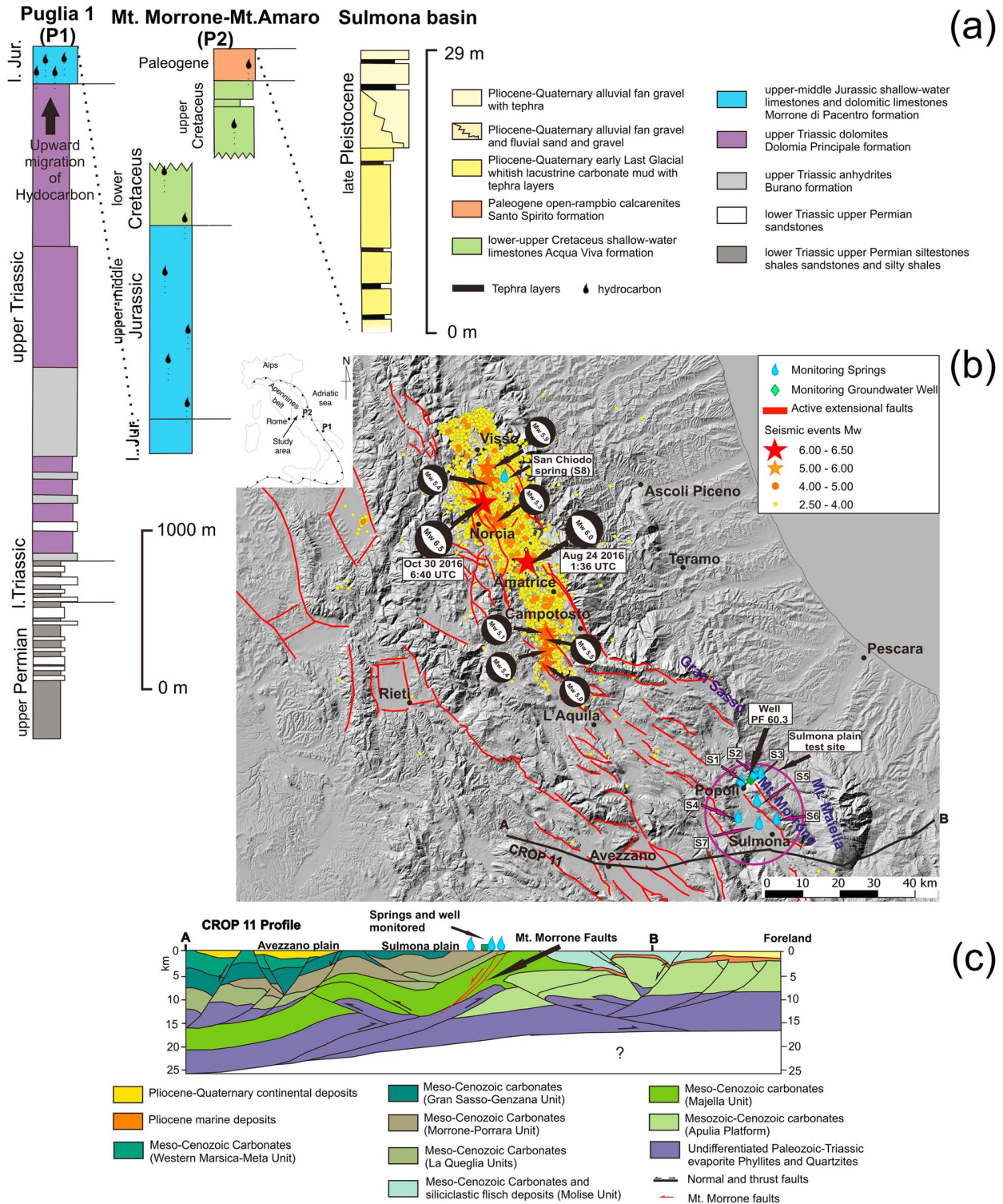


Figure 1. (a) Synthesis of stratigraphic logs from the Apulian-Adriatic foreland of the Apennines fold-thrust belt. See the well location in the upper-right inset of (b). (b) Map of central Apennines (see location in upper-left inset) showing earthquake epicenters of the 2016 to 2017 sequence. Locations of the monitoring well and springs analyzed in this work are displayed by blue drops and green squares, respectively. Earthquake epicenters are from the INGV database (available online at <http://cnt.rm.ingv.it/>). Active faults (red lines, all extensional) are from the Ithaca database (available online at <http://www.isprambiente.gov.it/en/projects/soil-and-territory/italy-hazards-from-capable-faulting>). (c) Interpretation of the CROP-11 deep seismic profile (modified after Patacca et al., 2008). See A-B profile track in (b). Note the location and depth of the extensional Mt. Morrone fault system (red faults) adjacent to the well and springs considered in this paper.

with deep CO₂ input. We present new data on boron isotope ratios that supports the potential role of elemental desorption from secondary solid phases (e.g., iron oxides and clays).

2. Setting

The Apennines (Figure 1) form a fold-thrust accretionary wedge that has progressively migrated eastward, toward the Adriatic foreland. Post-orogenic extension and normal faults have created numerous intramountain basins (Pliocene-Quaternary; Billi et al., 2006; Cavinato & DeCelles, 1999). In the study area (Sulmona plain; Figure 1b), located in the seismically active central Apennines (Galli et al., 2008), one of these extensional faults is the Mt. Morrone fault, striking NW-SE by roughly 25 km and dipping toward the SW by 50–60° (Figure 1c). This fault is considered to have been responsible for past earthquakes greater than Mw 6.5. Its most recent activation occurred during the second century Anno Domini (AD) (Ceccaroni et al., 2009; Galadini & Galli, 2001; Galli et al., 2008; Gori et al., 2011).

In the Sulmona area, the pre-orogenic succession consists of Meso-Cenozoic limestone and dolostone and Triassic evaporite with anhydrite and dolomite (units are thrust one over the other), as well as Permian-Triassic phyllite and quartzite (which makes up the crystalline basement; Parotto et al., 2003; Patacca et al., 2008). The fractured carbonates correspond to primary aquifers hosting regional groundwater flows (>10 m³/s from main springs) that converge from different hydrogeological units toward the study area. Minor springs are frequently characterized by mixing between regional flow and deep fluids, as in the sampled springs (Petitta et al., 2018). Moreover, two springs manifesting hydrocarbon seeps (Rusi et al., 2018) occur on the eastern side of Mt. Morrone. Source rocks consist of Upper Triassic layered or massive bituminous dolostone (Rusi et al., 2018). The syn-orogenic succession consists of hemipelagic marls overlain by sandstones with marl- and clay-rich interbeds (Brandano et al., 2010; Carminati et al., 2007), the latter of which correspond to the regional aquiclude. The post-orogenic deposits are mainly fluvial-lacustrine and gravel deposits (Quaternary), acting as aquitards with local groundwater flow. These deposits host well-preserved thin volcanoclastic layers (tephra), derived from the explosive activities of the peri-Tyrrhenian volcanoes or intra-Apennine centers (D'Orefice et al., 2006; Giaccio et al., 2013; Peccerillo, 2017; Figure 1a).

3. Data and Methods

The hydrogeochemical and hydrogeological data used in this work derive from the monitoring sites located in the Sulmona area (Barberio et al., 2017; Petitta et al., 2018) between the Gran Sasso and Morrone carbonate fractured aquifers, where regional groundwater flow paths converge to feed basal springs (Figure 1). The Morrone carbonate aquifer is bounded by low permeability layers; in the northern sector, these layers are constituted by the thrust zone between the Gran Sasso (top) and Mt. Morrone (bottom) carbonate units, where siliciclastic low-permeability deposits also outcrop. In the eastern sector, the low permeability limit is represented by the thrust zone between the Mt. Morrone unit (top) and the Laga siliciclastic flysch unit (bottom; Salvati, 2002); in the western sector, the Mt. Morrone active extensional fault partially isolates the deep carbonate aquifer from the local shallow aquifers located in the Plio-Quaternary continental clastic deposits of the Sulmona intramountain basin (Figure 1).

In this area, irregularly since July 2014 and systematically since January 2016, we hydrogeochemically monitored a group of seven springs fed both by the Mt. Morrone and by the Gran Sasso carbonate aquifers (Barberio et al., 2017; Petitta et al., 2018). The discharge area, corresponding to the Sulmona Plain and its northern prolongation (Popoli Gorges), receives groundwater flow both from regional aquifers, high and steady discharge springs, and locally from springs in the form of deep fluid contribution. The hydrogeological framework clearly indicates this area as a focal point of regional groundwater flow with deep flowpaths; for this reason, it is considered valuable for the monitoring aims of this research. Indeed, the stability of groundwater flow, showing minimal seasonal oscillations, allows for an optimal evaluation of groundwater changes due to reasons other than hydrogeological causes (i.e., seasonal recharge/discharge cycles, surface water/groundwater interaction, and lateral flow or leakage). The monitored springs were selected for their regime and chemical content as being representative of regional and deep groundwater flowpaths. These springs also exhibit hydrogeological and chemical stabilities, which indicates that the influence of seasonal and local hydraulic contributions is very limited and clearly identifiable (Barberio et al., 2017).

Samples from these springs were collected on a monthly basis. In particular, labile physical-chemical parameters (temperature and pH) were measured at the sampling site (Barberio et al., 2017), using a WTW Multi 3420 probe. New redox data (Eh in mV) measured from 28 April 2017 to 04 October 2017 using a WTW pH/Cond 3320 probe are shown in the supporting information Table S1. Water aliquots of the samples were analyzed in the laboratory for major cations, anions, and trace element content (along with $^{18}\text{O}/^{16}\text{O}$ and $^2\text{H}/^1\text{H}$ isotope ratios, here not discussed due to their nonsignificant variations; Barberio et al., 2017). Water aliquots for major and trace cations were acidified at 1% v/v by adding 65% p/p HNO_3 Suprapur® (Merck-Millipore). According to Standard Methods (Clesceri et al., 1999), the analytical accuracy on major ions ionic balance and on trace elements determination was better than 5%. The Limit of Quantification of As and V by inductively coupled plasma mass spectrometry (ICP-MS) was $0.01 \mu\text{g/L}$. We refer the reader to the previously published manuscript for further details on these analytical methods and on the statistical significance of As and V anomalies (Barberio et al., 2017). In this new study, new data elaborations and interpretations are furnished along with new B and Sr isotope analyses on selected samples.

The total dissolved solids (TDSs) are calculated by summing the concentrations (in milligrams per liter; Barberio et al., 2017) of the primary dissolved constituents as follows (Clesceri et al., 1999; Table S1):

$$\text{TDS} = [0.5 \times (\text{Alk as } \text{HCO}_3^-)] + \text{Ca}^{2+} + \text{Mg}^{2+} + \text{Na}^+ + \text{K}^+ + \text{Cl}^- + \text{SO}_4^{2-}.$$

In the Table S1, the molality concentrations, activities, and mineral saturation indexes (S.I.) of the sampled waters (Barberio et al., 2017) are calculated using the PhreeqcI code (Phreeqc Interactive), version 3, using the *llnl.dat* thermodynamic data set, which employs the Debye-Hückel theory for the activity calculation (Parkhurst & Appelo, 2013). Contrastingly, the *phreeqc.dat* data set was used for calculations at $P > 10^{-1}$ MPa (e.g., Figure 4). The total molality (molar per kilogram H_2O) of Ca, Mg, SO_4 , and C(4) = TDIC, resulting from speciation at the pH-T-P sampling conditions of spring water samples (Barberio et al., 2017), was used for the calculation of Ccarb and Cext parameters (Chiodini et al., 2000; Martini, 2016; Table S1).

The standard properties of hydrous ferric oxide (HFO, FeOOH) was used for surface complexation modeling (SCM; Dzombak & Morel, 1990; Parkhurst & Appelo, 2013; Zhu & Anderson, 2002): molecular formula weight = 89 g/mol; surface area = $600 \text{ m}^2/\text{g}$, strong site density = 0.005 mol/mol; weak site density = 0.2 mol/mol. Following adsorption modeling by the S3 water (17 December 2015 sample) and HFO surfaces at different equilibria conditions and weights, desorption was modeled by the infiltration of 16 (HFO sites coupled to ferrihydrite-water equilibria) or 20 (HFO weights: 0.25, 34, and 334 g) pore volumes, using the S1 water (17 December 2015 sample) as recharging water at increasing CO_2 fugacity (Parkhurst et al., 2011). Calcite saturation was fixed during modeling calculation (Data Set S1).

Boron ($^{11}\text{B}/^{10}\text{B}$) and strontium ($^{87}\text{Sr}/^{86}\text{Sr}$) isotope ratios were obtained by multicollector thermal ionization mass spectrometry (MC-TIMS) measurement (Triton, Thermo Scientific) at the University of Calgary (Elhamel, 2014; Wieser & Tuttas, 2009). Analyses were performed on $0.45\text{-}\mu\text{m}$ filtered S1 (both $^{11}\text{B}/^{10}\text{B}$ and $^{87}\text{Sr}/^{86}\text{Sr}$) and S8 (only $^{87}\text{Sr}/^{86}\text{Sr}$) samples, following column pretreatment to avoid an analytical background and taking into account the B and Sr concentrations. For boron, the delta values in permil of the isotope ratios ($\delta^{11}\text{B} \%$) were calculated against the reference material NIST SRM 951 (boric acid), whereas for strontium, ratios $^{87}\text{Sr}/^{86}\text{Sr}$ were normalized to NIST SRM 987 (strontium carbonate). The external reproducibility (2σ) was better than $\pm 2\%$ for $\delta^{11}\text{B}$ and ± 0.00002 for $^{87}\text{Sr}/^{86}\text{Sr}$. The results are shown in the final sheet of Table S1. A more detailed discussion of the methodology can be found in Supporting Information S1 (Barbieri et al., 2005, 2017; Bethke, 2008; Blanc et al., 2012; McArthur et al., 2012; Giaccio et al., 2013; Boschetti et al., 2017).

4. Modeling Pre-Seismic and Co-Seismic Geochemical Processes

4.1. "Deep CO_2 " Input

The involvement of deep CO_2 -bearing fluids in the triggering of earthquake sequences has been widely debated (Miller, 2013; Weinlich, 2014). A carbon mass balance of the involved water describing the origin of total dissolved inorganic carbon (TDIC) can be represented as follows (amounts expressed as m = molality; see the Supporting Information S1 for details) (Chiodini et al., 2000):

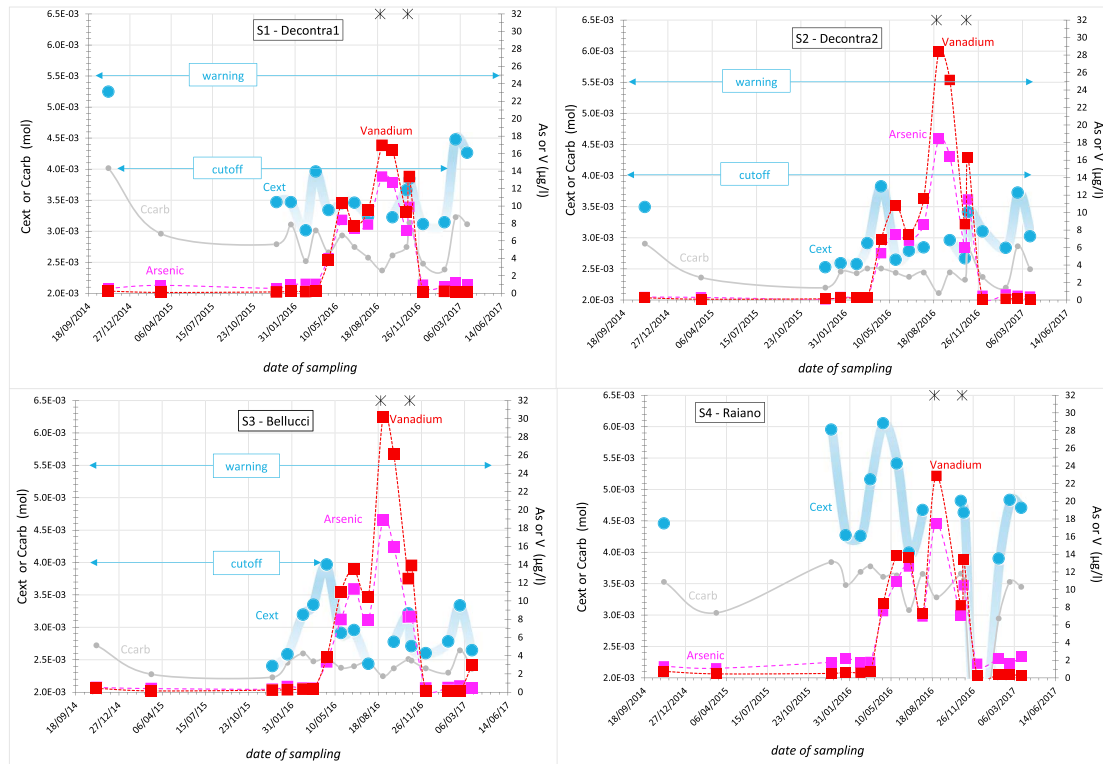


Figure 2. Time series for Cext-Ccarb (big blue-small gray dots joined by solid lines) and As-V (pink-red squares joined by dashed lines) of the S1–S4 springs. The dimension of the data points is greater than analytical accuracy (5%). Cutoff and warning threshold refer to Cext values of 4.0E-03 and 5.5E-03 m, respectively (Chiodini et al., 2004; Martini, 2016). These values are purely indicative and only shown for comparison. Cext gaps are due to a lack of pH data. Asterisks (*) denote $M_w \geq 5.0$ primary shock events: 24 August 2016 ($M_w = 6.0$) and 30 October 2016 ($M_w = 6.5$).

$$TDIC = Ccarb + Cext,$$

$$Ccarb = Ca + Mg-SO_4,$$

$$Cext = TDIC - Ccarb = Cinf + Cdeep.$$

Ccarb is the amount of carbon derived from the interaction of groundwater with carbonate aquifer rocks, while Cext is carbon derived from processes other than these (i.e., from external sources). This latter component can be expressed as $Cext = Cinf + Cdeep$, where Cinf is the carbon from atmospheric and biogenic CO₂ (infiltrating water) and Cdeep is deep CO₂ from metamorphism, mantle, or magma sources (Chiodini et al., 2000).

In previous studies conducted in the Central Italy, the following thresholds were proposed (Chiodini et al., 2000; Chiodini et al., 2004): $2.0E-03 \leq Cinf < 4.0E-03$ m. The low concentration concerns the waters with carbon mainly from a biogenic source (the background), whereas the high concentration is the threshold for the waters with important contribution of deep carbon (the “cutoff”; that is, the probability that this value is exceeded by Cinf is less than 1%; Chiodini et al., 2004). More recently, $Cinf = 2.31E-03 \pm 6.1E-04$ m has been proposed as representative of the recharge waters of the Apennines (Fron dini et al., 2018).

The easternmost sector of the Apennines has been considered as an area where the probability of finding groundwater with Cext greater than the cutoff is low (Chiodini et al., 2004). Consistent with this notion, the monthly sampling sequence of the S5 to S7 water samples collected in the study area prior to and during the seismic sequence shows a negligible excess of deep CO₂, that is, $Cext \approx Ccarb \approx Cinf$. In contrast, S1 to S4 waters show an increased input in deep carbon source up to the cutoff value, along with an arsenic-vanadium concentration jump (April 2016; Figures 2 and 3). Three statistic tests performed on S1–S4 springs have verified that the mean Cext detected during the sampling period is statistically different from the mean Cinf of the Apenninic recharging water (Fron dini et al., 2018; Tables 1 and S1–S4).

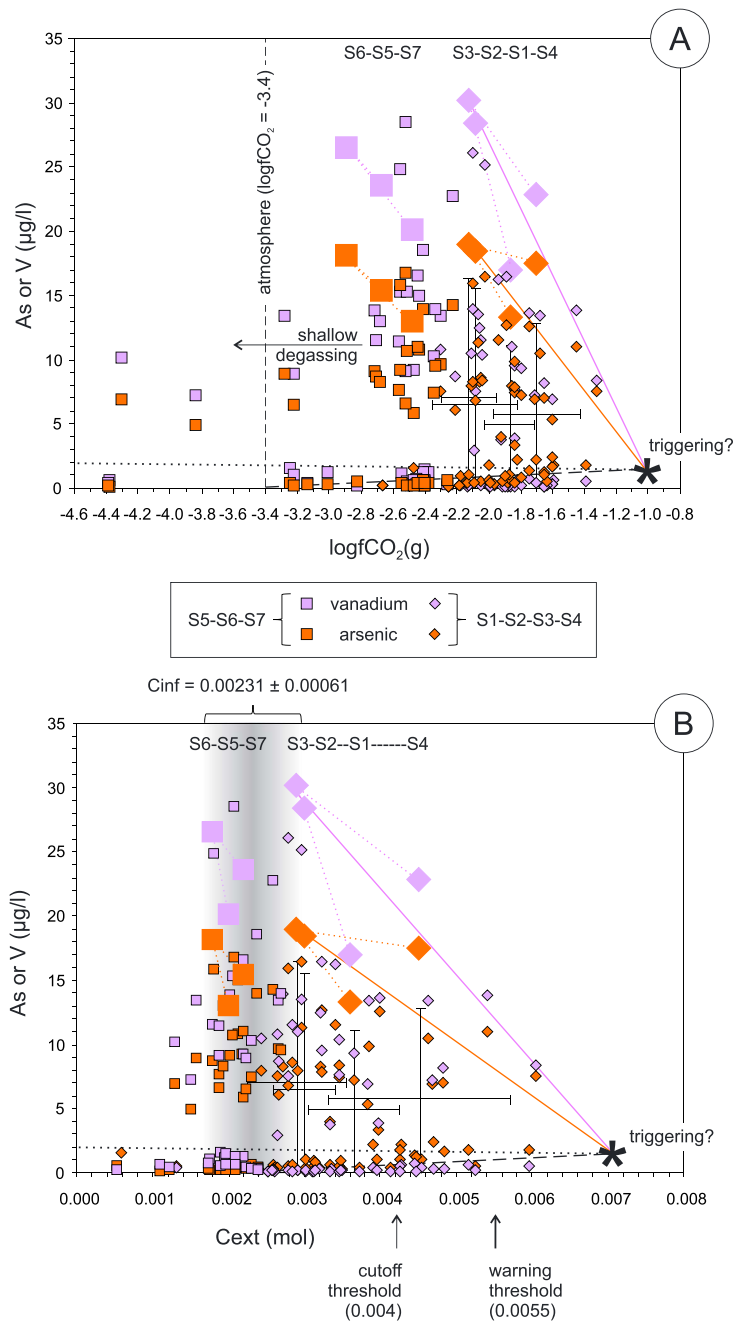


Figure 3. Arsenic (purple) and vanadium (orange) concentrations ($\mu\text{g/L}$) versus the calculated dissolved CO_2 fugacity as $\log f\text{CO}_2(\text{g})$ (a) and Cext molality (b). Oxidic-suboxic ($E_h \leq 0$: S1, S2, S3, S4; hereafter, S1 to S4) and oxidic ($E_h \geq 0$: S5, S6, S7; hereafter S5 to S7) sampled waters are distinguished by diamond and square symbols, respectively. The larger symbols depict the highest As-V concentration detected during the first seismic mainshock (24 August 2016). Unfortunately, it was not possible to calculate the Cext value for this period, due to a lack of pH values. For this reason, the larger symbols were plotted using the averaged Cext values (crosses indicate the mean \pm standard deviation of Cext for S1 to S4). The back extrapolation of the trend lines that approximately fit the higher As-V concentrations detected in the S1 to S4 samples (colored solid lines) intersects the CO_2/Cext buildup (dashed black line) at the following supposed desorption triggering values: As and V $\approx 2 \mu\text{g/L}$ (dotted black line), $\text{Cext} \approx 0.007 \text{ mol}$, and $\log f\text{CO}_2 \approx -1$. All sampled water is fresh (total dissolved solid $< 1 \text{ g/L}$) and has a Ca-HCO_3 main chemical composition. In comparison to the S5 to S7 spring group ($5 < \text{SO}_4 < 30 \text{ mg/L}$), the S1–S4 group is more enriched in dissolved sulfate ($40 < \text{SO}_4 < 180 \text{ mg/L}$), due to interaction with gypsum and anhydrite of the Upper Triassic fm. Moreover, all spring water shows a slight calcite oversaturation. This can be theoretically explained by a shift to the left in the following reaction:

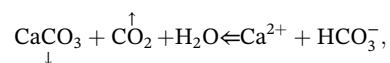
Table 1
Main Input Parameters and Results of the Two-Sample *T* Tests and *Z* Test (McDonald, 2014)

	Mean	Std. dev.	<i>N</i>	Rejection of the null hypothesis H_0 ($H_0 = \text{mean}_{\text{Cinf}} - \text{mean}_{\text{S\#}} = 0$) at $\alpha = 0.05^{\text{a}}$
Cinf	2.31E-03	6.10E-04	83	—
S1	3.65E-03	5.93E-04	16	Yes
S2	3.00E-03	2.88E-03	16	Yes
S3	2.82E-03	5.72E-04	16	Yes
S4	4.52E-03	1.26E-03	15	Yes

Note. Values in molality, *N* = sample size, Cinf from Frondini et al. (2018). Details are in Tables S1–S4.

^aChecked by the following three tests: Student's *T* test (equal variance), Welch's *T* test (unequal variance), and *Z* test.

Moreover, $\text{Cext} > \text{cutoff}$ is also detected. In particular, spring S4 shows (i) the most significant inverse relation between pH and Cext; (ii) Cext consistently above the threshold prior to the seismic sequence; (iii) two Cext values above $5.5\text{E-}03$ m, an early warning signal of possible seismic activity in the central Apennines (Martini, 2016), detected prior to As and V increase; and (iv) an abrupt Cext decrease following the seismic sequence, likely related to dilution after fracture opening, as confirmed by the decrease of the TDSs from higher than 400 mg/L down to 181 mg/L (TDS, Table S4-Raiano). The deep origin of the CO_2 along with the highest $\log f\text{CO}_2(\text{g}) = -1.3$ detected in S4 on 21 April 2016 supports the hypothesis of fluid pockets with high CO_2 pressure at crustal depths (Fabrizio et al., 2008). It also supports results from a previous study performed after the 2009 L'Aquila earthquake (Chiodini et al., 2011), that is, $\text{Cext} = 5.3\text{E-}03 \pm 2.9\text{E-}04$ m, $\delta^{13}\text{C}(\text{Cext}) = -8.31 \pm 0.64\text{‰}$. In contrast, the Cext values below or near to the cutoff threshold combined with an alkaline pH close to the water-atmospheric CO_2 -calcite equilibria ($\text{pH} = 8.2$ at $T = 13^\circ\text{C}$) are likely related to shallow CO_2 degassing and calcite precipitation (e.g., S2 water in Figures 3 and 4). Indeed, according to Frondini et al. (2018), the location of the Cext peak values in Figure 2 between the cutoff value and the recent defined limit of $\text{Cext} = 0.03$ m could be induced by these effects. Therefore, the thresholds depicted in Figures 2–4 are purely indicative and necessitate a local redefinition by a systematic inspection of the $\delta^{13}\text{C}$ values.



which depicts calcite precipitation (downward arrow), as supported by travertine deposition in the area (Carrara, 1998; Lombardo et al., 2001), and CO_2 loss at the spring outpouring (upward arrow). As a primary consequence, such combined carbon sinks produce both a pH increase and $\log f\text{CO}_2(\text{g})$ or Cext depletion. These effects are primarily represented by the S5 to S7 spring waters, which show $\log f\text{CO}_2(\text{g})$ values lower than at the atmospheric level (-3.4 ; “shallow degassing” in the A diagram), as well as Cext within the Cinf range (0.00231 ± 0.00061 ; Frondini et al., 2018; B diagram). Cutoff and warning threshold as in Figure 2.

4.2. Desorption

Arsenic and vanadium are redox sensitive elements that can exist between -3 to $+5$ and $+2$ to $+5$ oxidation states, respectively. As($+3$)-As($+5$) and V($+4$)-V($+5$) are the most important species in natural waters. Unfortunately, only aftershock redox potential data are available. These data include $-0.2 < \text{Eh} \leq 0$ volts for S1–S4 (compatible with the presence of dissolved sulfides) and $\text{Eh} \geq 0$ volts for S5–S7 (Table S1). Within these ranges of values, As and V mobility can be significantly reduced due to precipitation as oxides and sulfides, respectively, and/or via adsorption on iron oxide-hydroxide phases (Figure S1, Eh-pH diagram). However, by plotting the concentrations of As versus V detected in the studied groundwater prior to and during primary shocks, a general trend compatible with an oxic-suboxic (Wright et al., 2014) environment is shown in all the sampled springs (Figure 5). A stress-activated oxidation process at the water-rock interface may serve as an explanation for the observed common redox trend (Balk et al., 2009; Grant et al., 2011; Paudel et al., 2018; Singh et al., 2010). Moreover, the combined elemental increase may be the result of desorption from minerals' surface as iron oxide-hydroxides.

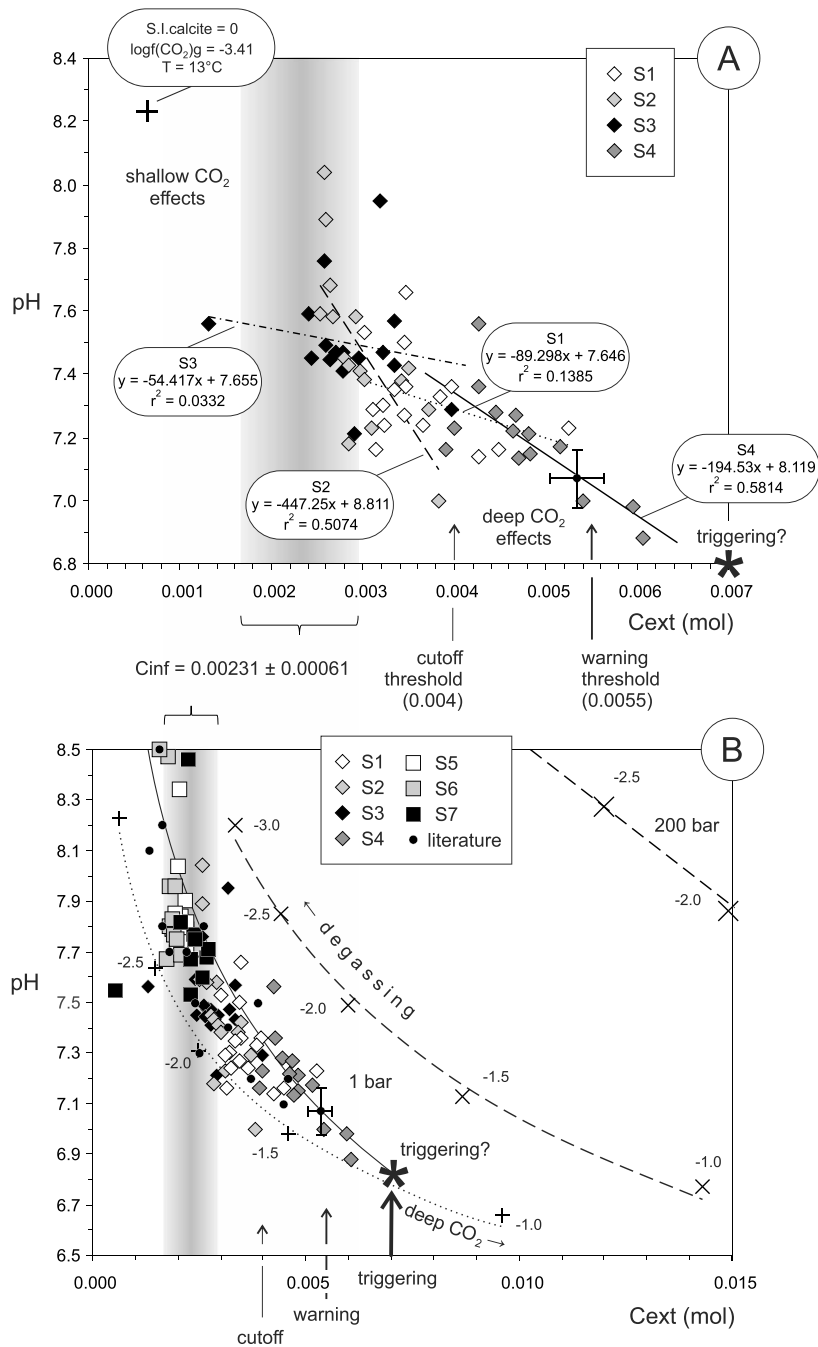


Figure 4. pH ($-\log[H^+]$) versus Cext (molality) calculated from total inorganic carbon. In (a), the linear best fits of water samples S1 to S4 are shown. In (b), all sampled waters, S1 to S4 and S5 to S7, are compared with water-CO₂ equilibria at $T_{\text{average}} = 13^\circ\text{C}$, $P = 10^{-1}$ MPa, and different $\log f\text{CO}_2$ values (+numbered and dotted best-fit curve). The black small dots show the composition of the Sulmona basin groundwater, as found in the literature (Conese et al., 2001; Iride, 2008). In both diagrams, the values detected in the S4 spring following the L'Aquila 2009 earthquake are also shown (black small dot with mean \pm standard deviation bars; Chiodini et al., 2011). Cinf (gray field) and cutoff-warning Cext thresholds (arrows) are shown for comparison (see main text for details; Chiodini et al., 2000; Frondini et al., 2018; Martini, 2016) along with the inferred desorption triggering value (Cext = 0.007 mol; Figure 3). In (b), the dashed curve represents the pH-Cext exponential best fit of a high CO₂ water issuing from a deep borehole in the Northern Apennine watershed (Bicocchi et al., 2013). The deep borehole draws fluid from a reservoir in the Upper Triassic rocks (Bicocchi et al., 2013). In this case, the equilibria between dissolved constituents and gases are first calculated at the temperature and pressure values at depth ($T = 120^\circ\text{C}$ and $P = 69$ MPa). Second, shallow degassing is simulated, recalculating the water-gas equilibria by decreasing the $\log f\text{CO}_2$ (X numbered and dashed best fit curve) at the same average conditions of the water sampled in this study (S.I.calcite = 0, $T_{\text{average}} = 13^\circ\text{C}$ and $P = 10^{-1}$ MPa). As a comparison, the same calculation at $P = 20$ MPa is also shown (X numbered and dashed best fit line). The solid curve shows that the exponential best fit for the S4 samples extends to higher and lower pH values.

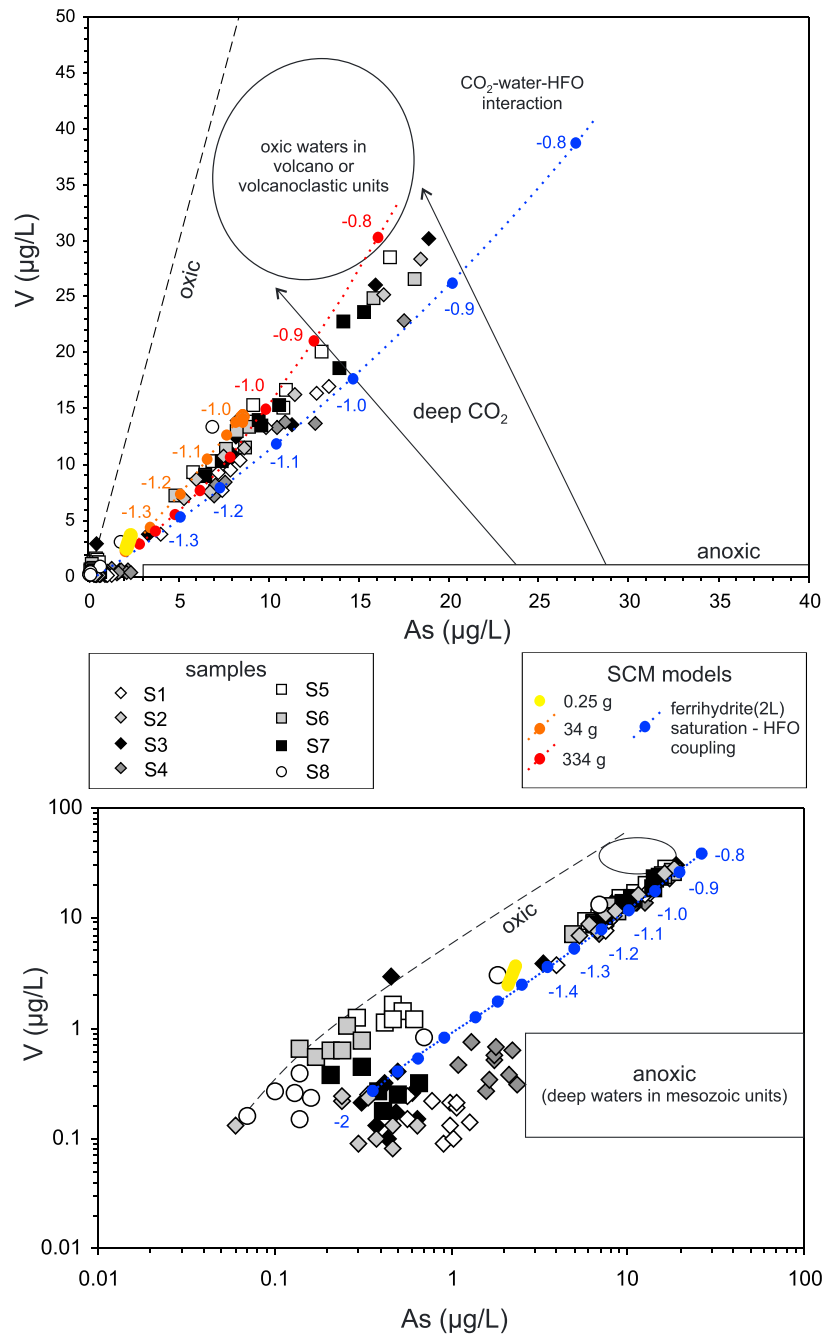


Figure 5. Vanadium and arsenic concentrations in the sampled water. Colored dotted lines show SCM desorption models (see text for explanation) at different HFO amounts or equilibria conditions (key) and logfCO₂ (numbers and dots). Oxic water fitting (Wright et al., 2014) (dashed black line), oxic water from volcanoclastic units (Sappa et al., 2014; circled field), and anoxic thermal fluids (Boschetti et al., 2005; squared field) are also shown for comparison. SCM = surface complexation modeling; HFO = hydrous ferric oxide.

The V and As concentrations from the interaction between water and surface minerals were calculated via SCM, using PhreeqcI computer code (Parkhurst & Appelo, 2013) version 3, applying a double-layer approach, and employing the *minteq.v4.dat* thermodynamic data set. Additional surface complexation constants for dissolved inorganic carbon and iron species from the *wateq4f.dat* data set were also included in the calculations. The desorption process of the adsorbed elements on HFO (HFO, FeOOH) was inferred by first

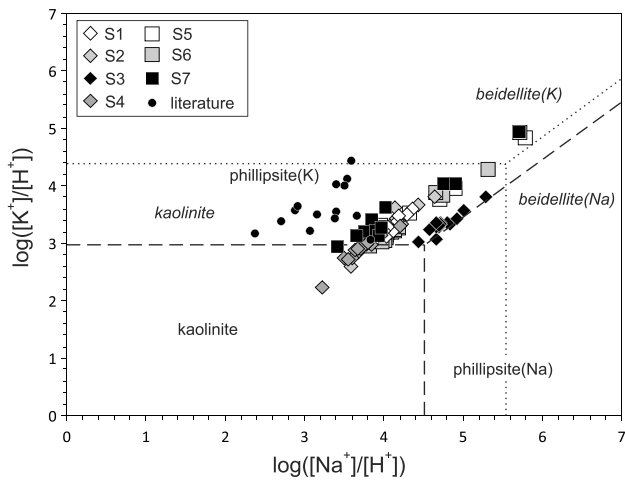


Figure 6. Activity diagrams for the system $\text{Na}_2\text{O-K}_2\text{O-Al}_2\text{O}_3\text{-SiO}_2\text{-H}_2\text{O}$ at $T = 13\text{ }^\circ\text{C}$ and $P = 10^{-1}\text{ MPa}$. Dissolved silica is saturated by cristobalite according to the equilibria calculated by using historical data regarding the S1 spring ($\text{SiO}_2 = 12\text{ mg/L}$; Popoli-SPA, 2018). The diagrams are drawn using the Act2 tool of the Geochemist's Workbench code, 7.0.2 release (Bethke, 2008). Lines show the theoretical equilibria between kaolinite and zeolites by using two different thermodynamic databases, thermo.com.v8.r6+.dat (dotted lines and the names of phases in italics; data set enclosed in the software) and gwb_thermodem_lv12_no-org_06jun17.dat, respectively (dashed lines). Literature data as in Figure 4b. The clustering of the sampled waters is parallel to the zeolites equilibria, in particular for S3, showing the highest As-V concentration during the first mainshock. It is worth noting that cristobalite, kaolinite, and zeolites are the typical weathering products of volcanic ashes and tephra (Bishop et al., 1998).

equilibrating a local water sample taken during the preseismic event with HFO and then providing an ingress of recharging water in the system in a similar manner to advective transport. In this second step, increasing values of CO_2 fugacity and fluid-calcite equilibria were set ($S.I.\text{-calcite} = 0$).

The results of the calculated modeling are comparable with the As-V trend depicted by the sampled waters, in particular (i) at high HFO amounts and (ii) if the HFO is connected to the ferrihydrite saturation of the first solution (Figure 5).

From the top (Quaternary alluvial deposits) to the bottom (Paleozoic basement) of the stratigraphic sequence, the adsorbent-desorbent secondary phases (i.e., iron oxide-hydroxides, clay minerals, and zeolites) can theoretically be formed from different siliciclastic sources (Figure 6).

Iron concentration in volcanic ash is highly variable, from lower than 1% as ferrihydrite in soil (andisol; Colombo et al., 2014) to very high amounts in deeper/older deposits (65% to 70% as opaque minerals; Bernoulli et al., 2004). Therefore, since published chemical data primarily concern iron from the unaltered solid fraction, the true concentration of ferrihydrite in local tephra layers is often difficult to determine. However, taking into account the available chemical composition (Galli et al., 2015), porosity (Macedonio & Costa, 2012; 67.5%), and density (Giaccio, 2006; 1.4 g/cm^3) of the tephra layers, a minimum HFO concentration of approximately 0.25 g/L , which may correspond to a heavily weathered andisol, can be inferred (Zhu & Anderson, 2002). Using this HFO amount, the desorbed As and V concentrations obtainable from the model are not higher than 2.3 and $3.7\text{ }\mu\text{g/L}$, even if a $\log_f(\text{CO}_2)_g = -1$ was entered. If the HFO amount is increased (e.g., supposing that all available iron was ferrihydrite or a similar amorphous phase, i.e., approximately 34 g), the calcu-

lated model paths expand (Figure 5). Furthermore, the greater the CO_2 fugacity, the more the model path matches the real samples. Finally, the reliability of our theory is supported by the following evidence (Figure 5): the highest As-V- CO_2 values of both modeling results and spring water data tend toward the field representing a potential analog site for peak concentrations in the westernmost Apennine sector (Sappa et al., 2014). Indeed, in this latter area, deep CO_2 -bearing groundwater continuously interacts with secondary minerals of the local volcanoclastic deposit (Battistel, 2014; circled area in Figure 5).

Regardless of the interaction with local tephra layers, the similarity between HFO-desorption models and As-V increase in groundwater during seismic events may have an alternative explanation. The accumulation of iron compounds in fault systems and their possible impact on groundwater composition, including radium and radon concentration (Szabo & Zapezca, 1993), has been highlighted several times in the literature (Boullier et al., 2004; Corrigan, 1998; Lipfert et al., 2006; Schuessler et al., 2016; Wang et al., 2017). Locally, the relationship between HFO and groundwater can be explained by an accumulation of amorphous iron hydroxide coatings on fault surfaces, or in fault gouges of the Mesozoic evaporite, rather than as a result of water-rock interaction with tephra layers, which are locally found no deeper than $\sim 100\text{ m}$ (Giaccio et al., 2013; Figure 1a). The substantially invariable strontium isotope ratio of the S1 spring ($0.70791\text{--}0.70794$; Figure S2) agrees with an interaction of water with Mesozoic carbonates/sulfates, rather than with Holocene ash layers ($0.7083\text{--}0.7112$; Figure S2; Giaccio et al., 2013). Accordingly, iron oxides can also be derived from the siliciclastic Verrucano unit (Permian-Lower Triassic; Parotto et al., 2003), which overlies the crystalline basement, and also occurs as fragments incorporated in the Upper Triassic sequence during the Alpine orogeny (Boschetti et al., 2017). Consequently, in this latter scenario, deep CO_2 and the As-V anomalies may be related to a deep origin.

The boron data independently support the hypothesis of elemental desorption from secondary minerals. The boron desorption concentration obtainable from SCM can vary significantly due to wide uncertainty in $\log K$ values describing strong sites' HFO-borates complexation: from 0.62 in the original *minteq.v4.dat*

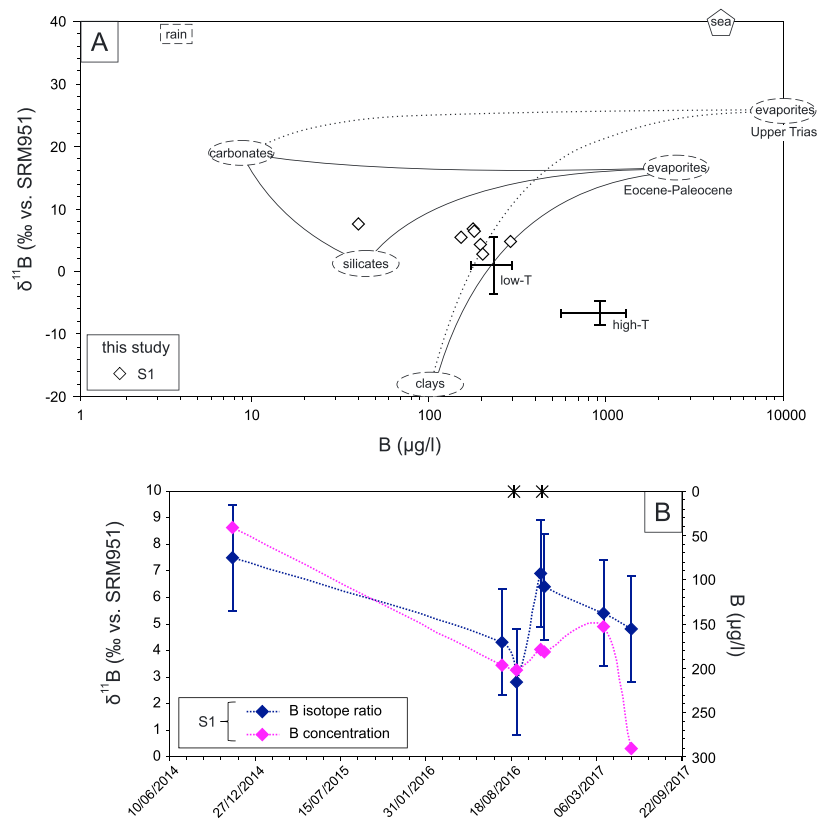


Figure 7. (a) $\delta^{11}\text{B}$ versus boron concentrations in the S1 water collected during the seismic sequence (data in Table S1). Dashed-contoured circles depict different and common boron sources (Barth, 1997; Négrel et al., 2009); solid and dotted lines represent the binary mixing between them. Crosses highlight the mean and standard deviation values detected in hot and cold water from volcanoclastic deposits (Battistel, 2014). (b) Time series of boron concentration and its isotope ratio $\delta^{11}\text{B}$ in S1 spring water. Error bars depict the external reproducibility of the $\delta^{11}\text{B}$ measurements at $\pm 2\%$ (2σ). Asterisk meaning as in Figure 2.

to 5.63 in the literature (Ranjbar & Jalali, 2014). However, by using the former (lower) value included in the data set, the B concentration increase due to desorption, as inferred by the models, is coherent with that detected in the groundwater samples (Data Set S1). In a similar manner and consistently with the total chromium increase during the seismic event, the Cr concentration in the groundwater desorbed after SCM shows an increment of at least 10 times compared to the initial groundwater concentration (Data Set S1).

It is worth noting that the simultaneous boron concentration increase and boron isotope ratio decrease (from 40 to 290 $\mu\text{g/L}$ and from $\delta^{11}\text{B} = +7.5\%$ to $\delta^{11}\text{B} = +2.8\%$, respectively), exhibited by the S1 water samples prior to the seismic events, may be related to desorption from mineral surfaces (Figure 7). This desorption process is supported by the following considerations: (i) clays and iron oxides-(hydroxides) logK values (Ranjbar & Jalali, 2014) and isotope fractionation effects (^{10}B enrichment on the surface of minerals; Lemarchand et al., 2007; Schwarcz et al., 1969) are similar; (ii) similar boron concentration and $\delta^{11}\text{B}$ values were detected in cold groundwater, which interacted with clays and/or iron hydroxides formed in volcanic deposits ($B = 233 \pm 58 \mu\text{g/L}$; $\delta^{11}\text{B} = +0.9 \pm 4.5\%$; Battistel, 2014). Finally, the hypothesis of boron desorption is in agreement with previous work concerning different boron sources (Barth, 1997; Négrel et al., 2009; Figure 7).

5. Conclusions

In this study, we assessed the possible relationship between deep CO_2 inflow and the anomalies on trace elements such as arsenic (As) and vanadium (V) detected in groundwater before and during the 2016

earthquakes in central Italy. SCM shows that both As and V release can be related to ubiquitous secondary mineral phases as iron oxides and triggered by deep CO₂ dissolved in the water. While the As and V concentration anomalies were significant and have been verified at most of the monitored springs, the possible concomitant boron (B) desorption processes necessitate further analyses to prove that a similar isotopic signature occurred in other groundwater sampling sites. However, the analysis of boron (B) concentration and isotope ratio at one spring provides tentative confirmation that the desorption processes occurred from alteration minerals on volcanoclastic deposits. The combined role of deep CO₂ and elemental desorption processes could open new perspectives in strategies concerning the identification of seismic precursors.

Author Contributions

T. B., M. B., M. P., A. B., and M. D. B. formulated the original hypotheses and designed and developed the research project. M. B., M. D. B., A. B., S. F., and M. P. collected samples, performed research, and participated in the data analysis and data interpretation. T. B. and M. B. performed hydrogeochemical modeling with insights from all authors. All authors discussed the data presented in the manuscript and participated in its writing and in the figure-table preparation. Authors declare no financial conflicts of interests. All data used for this paper are available in Table 1, in Figures S1 and S2, and in two files (Table S1 and Data Set S1; *Boschetti et al. Supporting Tables.xlsx* and *Boschetti et al. Supporting Model Results.xlsx*) associated with the supporting information. Authors declare solely institutional funding from their institutions.

Acknowledgments

We would like to thank the Editor, M. Edmonds, Associate Editor, F. Cooper, and Reviewers, G. De Luca and A. Skelton, for careful reading, valuable comments, and constructive suggestions, which helped to improve the quality of the manuscript.

References

- Andr n, M., Stockmann, G., Skelton, A., Sturkell, E., M rth, C. M., Gu r nard ttir, H. R., et al. (2016). Coupling between mineral reactions, chemical changes in groundwater, and earthquakes in Iceland. *Journal of Geophysical Research: Solid Earth*, 121, 2315–2337. <https://doi.org/10.1002/2015JB012614>
- Balk, M., Bose, M., Ertem, G., Rogoff, D. A., Rothschild, L. J., & Freund, F. T. (2009). Oxidation of water to hydrogen peroxide at the rock–water interface due to stress-activated electric currents in rocks. *Earth and Planetary Science Letters*, 283, 87–92.
- Barberio, M. D., Barbieri, M., Billi, A., Doglioni, C., & Petitta, M. (2017). Hydrogeochemical changes before and during the 2016 Amatrice–Norcia seismic sequence (central Italy). *Scientific Reports*, 7(1), 11,735. <https://doi.org/10.1038/s41598-017-11990-8>
- Barbieri, M., Boschetti, T., Petitta, M., & Tallini, M. (2005). Stable isotope (2H, 18O and 87Sr/ 86Sr) and hydrochemistry monitoring for groundwater hydrodynamics analysis in a karst aquifer (Gran Sasso, Central Italy). *Applied Geochemistry*, 20(11), 2063–2081. <https://doi.org/10.1016/j.apgeochem.2005.07.008>
- Barbieri, M., Nigro, A., & Petitta, M. (2017). Groundwater mixing in the discharge area of San Vittorino Plain (Central Italy): Geochemical characterization and implication for drinking uses. *Environmental Earth Sciences*, 76(11), 393. <https://doi.org/10.1007/s12665-017-6719-1>
- Barth, S. (1997). The boron isotope systematics of groundwater from crystalline basement and sedimentary aquifers (SW Germany - N Switzerland), Paper Presented at Seventh Annual V. M. Goldschmidt Conference, European Association of Geochemistry and Geochemical Society, Tucson, Arizona, USA.
- Battistel, M. (2014). Utilizzo di traccianti geochimici per lo studio del sistema idrotermale a bassa entalpia del distretto vulcanico Cimino-Vicano: stima della risorsa e implicazioni ambientali., Sapienza University of Rome.
- Bernoulli, D., Schaltegger, U., Stern, W. B., Frey, M., Caron, M., & Monechi, S. (2004). Volcanic ash layers in the Upper Cretaceous of the Central Apennines and a numerical age for the early Campanian. *International Journal of Earth Sciences*, 93(3), 384–399. <https://doi.org/10.1007/s00531-004-0389-4>
- Bethke, C. M. (2008). *Geochemical and biogeochemical reaction modeling*, (Second ed.). New York: Cambridge University Press.
- Bicocchi, G., Tassi, F., Bonini, M., Capeccchiacci, F., Ruggieri, G., Buccianti, A., et al. (2013). The high pCO₂ Caprese Reservoir (Northern Apennines, Italy): Relationships between present- and paleo-fluid geochemistry and structural setting. *Chemical Geology*, 351, 40–56. <https://doi.org/10.1016/j.chemgeo.2013.05.001>
- Billi, A., Tiberti, M. M., Cavinato, G. P., Cosentino, D., Di Luzio, E., Keller, J. V. A., et al. (2006). First results from the CROP-11 deep seismic profile, central Apennines, Italy: Evidence of mid-crustal folding. *Journal of the Geological Society, London*, 163(4), 583–586. <https://doi.org/10.1144/0016-764920-002>
- Bishop, J. L., Fr schl, H., & Mancinelli, R. L. (1998). Alteration processes in volcanic soils and identification of exobiologically important weathering products on Mars using remote sensing. *Journal of Geophysical Research*, 103(E13), 31457–31476. <https://doi.org/10.1029/1998JE900008>
- Blanc, P., Lassin, A., Piantone, P., Azaroual, M., Jacquemet, N., Fabbri, A., & Gaucher, E. C. (2012). Thermodem: A geochemical database focused on low temperature water/rock interactions and waste materials. *Applied Geochemistry*, 27(10), 2107–2116. <https://doi.org/10.1016/j.apgeochem.2012.06.002>
- Bolliger, C., H hener, P., Hunkeler, D., H berli, K., & Zeyer, J. (1999). Intrinsic bioremediation of a petroleum hydrocarbon-contaminated aquifer and assessment of mineralization based on stable carbon isotopes. *Biodegradation*, 10(3), 201–217. <https://doi.org/10.1023/A:1008375213687>
- Boschetti, T., Toscani, L., Barbieri, M., Mucchino, C., & Marino, T. (2017). Low enthalpy Na-chloride waters from the Lunigiana and Garfagnana grabens, Northern Apennines, Italy: Tracing fluid connections and basement interactions via chemical and isotopic compositions. *Journal of Volcanology and Geothermal Research*, 348, 12–25. <https://doi.org/10.1016/j.jvolgeores.2017.10.008>
- Boschetti, T., Venturelli, G., Toscani, L., Barbieri, M., & Mucchino, C. (2005). The Bagni di Lucca thermal waters (Tuscany, Italy): An example of Ca-SO₄ waters with high Na/Cl and low Ca/SO₄ ratios. *Journal of Hydrology*, 307(1–4), 270–293. <https://doi.org/10.1016/j.jhydrol.2004.10.015>

- Boullier, A. M., Fujimoto, K., Ohtani, T., Roman-Ross, G., Lewin, E., Ito, H., & Ildefonse, B. (2004). Textural evidence for recent co-seismic circulation of fluids in the Nojima fault zone, Awaji island, Japan. *Tectonophysics*, 378(3–4), 165–181. <https://doi.org/10.1016/j.tecto.2003.09.006>
- Brandano, M., Corda, L., & Castorina, F. (2010). Facies and sequence architecture of a tropical foramol-rhodalg carbonate ramp: Miocene of the central Apennines (Italy). In M. Mutti, W. E. Piller, & C. Betzler (Eds.), *Carbonate systems during the Oligocene-Miocene climatic transition (IAS special publication)*, edited by, (pp. 107–128). The Atrium, Southern Gate, Chichester, West Sussex, UK: John Wiley & Sons Ltd.
- Carminati, E., Corda, L., Mariotti, G., & Brandano, M. (2007). Tectonic control on the architecture of a Miocene carbonate ramp in the Central Apennines (Italy): Insights from facies and backstripping analyses. *Sedimentary Geology*, 198(3–4), 233–253. <https://doi.org/10.1016/j.sedgeo.2006.12.005>
- Carrara, C. (1998). I travertini della Valle del Pescara tra Popoli e Torre dè Passeri. *Il Quaternario*, 11(2), 163–179.
- Cavinato, G. P., & DeCelles, P. (1999). Extensional basins in the tectonically bimodal central Apennines fold-thrust belt, Italy: Response to corner flow above a subducting slab in retrograde motion. *Geology*, 27(10), 955–958. [https://doi.org/10.1130/0091-7613\(1999\)027<0955:EBITTB>2.3.CO;2](https://doi.org/10.1130/0091-7613(1999)027<0955:EBITTB>2.3.CO;2)
- Ceccaroni, E., Ameri, G., Capera, A. A. G., & Galadini, F. (2009). The 2nd century AD earthquake in central Italy: Archaeoseismological data and seismotectonic implications. *Natural Hazards*, 50(2), 335–359. <https://doi.org/10.1007/s11069-009-9343-x>
- Chen, C. H., Tang, C. C., Cheng, K. C., Wang, C. H., Wen, S., Lin, C. H., et al. (2015). Groundwater–strain coupling before the 1999 Mw 7.6 Taiwan Chi-Chi earthquake. *Journal of Hydrology*, 524, 378–384. <https://doi.org/10.1016/j.jhydrol.2015.03.006>
- Chiaraluce, L., Di Stefano, R., Tinti, E., Scognamiglio, L., Monachesi, G., Lombardi, A., et al. (2017). The 2016 Central Italy seismic sequence: A first look at the mainshocks, aftershocks and source models. *Seismological Research Letters*, 88(3), 757–771. <https://doi.org/10.1785/0220160221>
- Chiodini, G., Caliro, S., Cardellini, C., Frondini, F., Inguaggiato, S., & Matteucci, F. (2011). Geochemical evidence for and characterization of CO₂ rich gas sources in the epicentral area of the Abruzzo 2009 earthquakes. *Earth and Planetary Science Letters*, 304(3–4), 389–398. <https://doi.org/10.1016/j.epsl.2011.02.016>
- Chiodini, G., Cardellini, C., Amato, A., Boschi, E., Caliro, S., Frondini, F., & Ventura, G. (2004). Carbon dioxide Earth degassing and seismogenesis in central and southern Italy. *Geophysical Research Letters*, 31, L07615. <https://doi.org/10.1029/2004GL019480>
- Chiodini, G., Frondini, F., Cardellini, C., Parello, F., & Peruzzi, L. (2000). Rate of diffuse carbon dioxide Earth degassing estimated from carbon balance of regional aquifers: The case of central Apennine, Italy. *Journal of Geophysical Research*, 105(B4), 8423–8434. <https://doi.org/10.1029/1999JB900355>
- Claesson, L., Skelton, A., Graham, C., Dietl, C., Mörth, M., Torssander, P., & Kockum, I. (2004). Hydrogeochemical changes before and after a major earthquake. *Geology*, 32(8), 641–644. <https://doi.org/10.1130/G20542.1>
- Clesceri, L. S., Greenberg, A. E., & Eaton, A. D. (1999). Method 1030 E, Checking correctness of analyses. In *Standard methods for the examination of water and wastewater*, edited. Washington: American Public Health Association, American Water Works Association, Water Environment Federation.
- Colombo, C., Sellitto, V. M., Palumbo, G., Di Iorio, E., Terribile, F., & Schulze, D. G. (2014). Clay formation and pedogenetic processes in tephra-derived soils and buried soils from Central-Southern Apennines (Italy). *Geoderma*, 213, 346–356. <https://doi.org/10.1016/j.geoderma.2013.08.005>
- Conese, M., Nanni, T., Peila, C., Rusi, S., & Salvati, R. (2001). Idrogeologia della Montagna del Morrone (Appennino Abruzzese): dati preliminari. *Memorie della Societa Geologica Italiana*, 56, 181–196.
- Corrigan, C. A. (1998). *Characterization of secondary minerals forming at fracture surfaces in aquitards (Saskatchewan, Ontario)*. Kingston, Ontario, Canada: Queen's University.
- De Luca, G., Di Carlo, G., & Tallini, M. (2018). A record of changes in the Gran Sasso groundwater before, during and after the 2016 Amatrice earthquake, central Italy. *Scientific Reports*, 8(1), 15,982. <https://doi.org/10.1038/s41598-018-34444-1>
- D'Orefice, M., Graciotti, R., Capitanio, F., Stoppa, F., Rosatelli, G., & Barbieri, M. (2006). Middle-Pleistocene volcanism in the Latium-Abruzzi Apennines: From scientific peculiarities to applicative aspects. *Memorie Descrittive della Carta Geologica d'Italia*, 72, 7–67.
- Dzombak, D. A., & Morel, F. M. M. (1990). *Surface complexation modeling: Hydrous ferric oxide*. New York: John Wiley & Sons.
- Elhamel, N. (2014). *The development of an analytical technique to measure stable and radiogenic strontium isotope ratios using thermal ionization mass spectrometry with the double spike method*, 91 pp. Calgary, Alberta: University of Calgary.
- Fabrizio, A., Mulch, A., Chamberlain, P., & Aydin, A. (2008). Geochemical traces of CO₂-rich fluid flow along normal faults in central Italy. *Geophysical Journal International*, 174(2), 758–770.
- Faluccci, E., Gori, S., Bignami, C., Pietrantonio, G., Melini, D., Moro, M., et al. (2018). The Campotosto seismic gap in between the 2009 and 2016–2017 seismic sequences of central Italy and the role of inherited lithospheric faults in regional seismotectonic settings. *Tectonics*, 37, 2425–2445. <https://doi.org/10.1029/2017TC004844>
- Frondini, F., Cardellini, C., Caliro, S., Beddini, G., Rosiello, A., & Chiodini, G. (2018). Measuring and interpreting CO₂ fluxes at regional scale: The case of the Apennines, Italy. *Journal of the Geological Society*, 176(2), 408–416.
- Galadini, F., & Galli, P. (2001). Archaeoseismology in Italy: Case studies and implications on long-term seismicity. *Journal of Earthquake Engineering*, 5(1), 35–68. <https://doi.org/10.1080/13632460109350385>
- Galli, P., Galadini, F., & Pantosti, D. (2008). Twenty years of paleoseismology in Italy. *Earth-Science Reviews*, 88(1–2), 89–117. <https://doi.org/10.1016/j.earscirev.2008.01.001>
- Galli, P., Giaccio, B., Peronace, E., & Messina, P. (2015). Holocene Paleoequakes and Early–Late Pleistocene Slip Rate on the Sulmona Fault (Central Apennines, Italy). *Bulletin of the Seismological Society of America*, 105(1), 1–13. <https://doi.org/10.1785/0120140029>
- Giaccio, B. (2006). L'eruzione dell'Ignimbrite Campana (c. 40 ka BP), oscillazioni climatiche sub-orbitali e i cambiamenti bioculturali dell'OIS 3 europeo, 164 pp, Università degli Studi di Napoli Federico II.
- Giaccio, B., Castorina, F., Nomade, S., Scardia, G., Voltaggio, M., & Sagnotti, L. (2013). Revised chronology of the Sulmona lacustrine succession, central Italy. *Journal of Quaternary Science*, 28(6), 545–551. <https://doi.org/10.1002/jqs.2647>
- Gori, S., Giaccio, B., Galadini, F., Faluccci, E., Messina, P., Sposato, A., & Dramis, F. (2011). Active normal faulting along the Mt. Morrone south-western slopes (central Apennines, Italy). *International Journal of Earth Sciences*, 100(1), 157–171. <https://doi.org/10.1007/s00531-009-0505-6>
- Grant, R. A., Halliday, T., Balderer, W. P., Leuenberger, F., Newcomer, M., Cyr, G., & Freund, F. T. (2011). Ground water chemistry changes before major earthquakes and possible effects on animals. *International Journal of Environmental Research and Public Health*, 8(6), 1936–1956. <https://doi.org/10.3390/ijerph8061936>

- Huang, F., Li, M., Ma, Y., Han, Y., Tian, L., Yan, W., & Li, X. (2012). Studies on earthquake precursors in China: A review for recent 50 years. *Geodesy and Geodynamics*, 8, 1–12.
- Igarashi, G., Saeki, S., Takahata, N., Sumikawa, K., Tasaka, S., Sasaki, Y., et al. (1995). Groundwater radon anomaly before the Kobe earthquake in Japan. *Science*, 269(5220), 60–61. <https://doi.org/10.1126/science.269.5220.60>
- Inan, S., Balderer, W. P., Leuenberger-West, F., Yakan, H., Ozvan, A., & Freund, F. T. (2012). Springwater chemical anomalies prior to the Mw = 7.2 Van earthquake (Turkey). *Geochemical Journal*, 46, 11–16.
- Ingebritsen, S. E., & Manga, M. (2014). Earthquakes: Hydrogeochemical precursors. *Nature Geoscience*, 7(10), 697–698. <https://doi.org/10.1038/ngeo2261>
- Iride, R. (2008-2009). *Idrogeologia applicata ed ambientale del Morrone Settentrionale*, 215 pp. Università degli Studi di "G. d'Annunzio" Chieti - Pescara.
- Lemarchand, E., Schott, J., & Gaillardet, J. (2007). How surface complexes impact boron isotope fractionation: Evidence from Fe and Mn oxides sorption experiments. *Earth and Planetary Science Letters*, 260(1–2), 277–296. <https://doi.org/10.1016/j.epsl.2007.05.039>
- Lipfert, G., Reeve, A. S., Sidle, W. C., & Marvinney, R. (2006). Geochemical patterns of arsenic-enriched ground water in fractured, crystalline bedrock, Northport, Maine, USA. *Applied Geochemistry*, 21(3), 528–545. <https://doi.org/10.1016/j.apgeochem.2005.12.001>
- Lombardo, M., Calderoni, G., D'Alessandro, L., & Miccadei, E. (2001). The travertine deposits of the upper Pescara valley (Central Abruzzi, Italy): A clue for the reconstruction of the late Quaternary Palaeoenvironmental evolution of the area. In G. Visconti, M. Beniston, E. D. Iannorelli, & D. Barba (Eds.), *Global Change and Protected Areas*, (pp. 459–464). New York, USA: Kluwer Academic Publishers. https://doi.org/10.1007/0-306-48051-4_42
- Macedonio, G., & Costa, A. (2012). Brief communication "rain effect on the load of tephra deposits". *Natural Hazards and Earth System Sciences*, 12(4), 1229–1233. <https://doi.org/10.5194/nhess-12-1229-2012>
- Martini, C. (2016). Signals in water—the deep originated CO₂ in the Peschiera-Capone aqueduct in relation to monitoring of seismic activity in central Italy. *Acque Sotterranee-Italian Journal of Groundwater*, 5(4). <https://doi.org/10.7343/as-2016-246>
- McArthur, J. M., Howarth, R. J., & Shields, G. A. (2012). Strontium isotope stratigraphy. In F. M. Gradstein, J. G. Ogg, M. D. Schmitz, & G. M. Ogg (Eds.), *The Geological Time Scale 2012* (pp. 127–144). Oxford: Elsevier B.V. <https://doi.org/10.1016/B978-0-444-59425-9.00007-X>
- McDonald, J. H. (2014). *Handbook of biological statistics*, (3rd ed.). Baltimore, Maryland: Sparky House Publishing.
- Miller, S. A. (2013). The role of fluids in tectonic and earthquake processes. In R. Dmowska (Ed.), *Advances in geophysics*, (pp. 1–46). San Diego, CA, USA: Elsevier.
- Négrel, P., Petelet-Giraud, E., & Brenot, A. (2009). Use of isotopes for groundwater characterization and monitoring. In P. Quevauviller, A. M. Fouillac, J. Grath, & R. Ward (Eds.), *Groundwater monitoring*, (pp. 331–354). The Atrium, Southern Gate, Chichester, West Sussex, UK: John Wiley and Sons, Ltd. <https://doi.org/10.1002/9780470749685.ch22>
- Parkhurst, D. L., and C. A. J. Appelo (2013). Description of input and examples for PHREEQC version 3—A computer program for speciation, batch-reaction, one-dimensional transport, and inverse geochemical calculations *Rep.*, 497 pp, U.S. geological survey, techniques and methods, book 6, chap. A43, <http://pubs.usgs.gov/tm/06/a43/>.
- Parkhurst, D. L., P. Glynn, and R. Johnson (2011). *Geochemistry for ground-water systems*, Edited, P. Workshop, USGS.
- Parotto, M., Cavinato, G. P., Miccadei, E., & Tozzi, M. (2003). Line CROP 11: Central Apennines. *Memorie descrittive della Carta Geologica d'Italia*, 62, 145–154.
- Patacca, E., Scandone, P., Di Luzio, E., Cavinato, G. P., & Parotto, M. (2008). Structural architecture of the central Apennines: Interpretation of the CROP 11 seismic profile from the Adriatic coast to the orographic divide. *Tectonics*, 27, TC3006. <https://doi.org/10.1029/2005TC001917>
- Paudel, S. R., Banjara, S. P., Wagle, A., & Freund, F. T. (2018). Earthquake chemical precursors in groundwater: A review. *Journal of Seismology*, 1-22, 1293–1314.
- Peccerillo, A. (2017). *Cenozoic volcanism in the Tyrrhenian Sea Region* (2nd ed.). CH-4052 Basel, Switzerland: Springer International Publishing AG. <https://doi.org/10.1007/978-3-319-42491-0>
- Petitta, M., Mastroiello, L., Preziosi, E., Banzato, F., Barberio, M. D., Billi, A., et al. (2018). Water-table and discharge changes associated with the 2016–2017 seismic sequence in central Italy: Hydrogeological data and a conceptual model for fractured carbonate aquifers. *Hydrogeology Journal*, 26(4), 1009–1026. <https://doi.org/10.1007/s10040-017-1717-7>
- Popoli-SPA (2018). Chemical composition of the DeContra sulfidic water, edited, pp. Terme di Popoli - University of Napoli "Federico II", Pharmacy Department.
- Ranjbar, F., & Jalali, M. (2014). Surface complexation model of boron adsorption by calcareous soils. *International journal of Environmental Science and Technology*, 11(5), 1317–1326. <https://doi.org/10.1007/s13762-014-0544-9>
- Rusi, S., Di Curzio, D., Palmucci, W., & Petaccia, R. (2018). Detection of the natural origin hydrocarbon contamination in carbonate aquifers (central Apennine, Italy). *Environmental Science and Pollution Research*, 25(16), 15577–15596. <https://doi.org/10.1007/s11356-018-1769-9>
- Salvati, R. (2002). Natural hydrogeological laboratories: A new concept in regional hydrogeology studies. A case history from central Italy. *Environmental Geology*, 41(8), 960–965. <https://doi.org/10.1007/s00254-001-0474-y>
- Sano, Y., & Wakita, H. (2016). Precise measurement of helium isotopes in terrestrial gases. *Bulletin of the Chemical Society of Japan*, 61, 1153–1157.
- Sappa, G., Ergul, S., & Ferranti, F. (2014). Geochemical modeling and multivariate statistical evaluation of trace elements in arsenic contaminated groundwater systems of Viterbo Area, (Central Italy). *Springerplus*, 3(1), 237. <https://doi.org/10.1186/2193-1801-3-237>
- Schuessler, J. A., Kämpf, H., Koch, U., & Alawi, M. (2016). Earthquake impact on iron isotope signatures recorded in mineral spring water. *Journal of Geophysical Research: Solid Earth*, 121, 8548–8568. <https://doi.org/10.1002/2016JB013408>
- Schwarz, H. P., Agyei, E. K., & McMullen, C. C. (1969). Boron isotopic fractionation during clay adsorption from sea-water. *Earth and Planetary Science Letters*, 6(1), 1–5. [https://doi.org/10.1016/0012-821X\(69\)90084-3](https://doi.org/10.1016/0012-821X(69)90084-3)
- Singh, R. P., Kumar, J. S., Zlotnicki, J., & Kafatos, M. (2010). Satellite detection of carbon monoxide emission prior to the Gujarat earthquake of 26 January 2001. *Applied Geochemistry*, 25(4), 580–585. <https://doi.org/10.1016/j.apgeochem.2010.01.014>
- Skelton, A., Andrién, M., Kristmannsdóttir, H., Stockmann, G., Mörrh, C. M., Sveinbjörnsdóttir, A., et al. (2014). Changes in groundwater chemistry before two consecutive earthquakes in Iceland. *Nature Geoscience*, 7(10), 752–756. <https://doi.org/10.1038/ngeo2250>
- Skelton, A., Claesson, L., Chakrapani, G., Mahanta, C., Routh, J., Mört, M., & Khanna, P. (2008). Coupling between seismic activity and hydrogeochemistry at the Shillong Plateau, Northeastern India. *Pure and Applied Geophysics*, 165(1), 45–61. <https://doi.org/10.1007/s00024-007-0288-2>

- Skelton, A., Liljedahl-Claesson, L., Wästeby, N., Andrén, M., Stockmann, G., Sturkell, E., et al. (2019). Hydrochemical changes before and after earthquakes based on long term measurements of multiple parameters at 2 sites in northern Iceland—A review. *Journal of Geophysical Research: Solid Earth*. <https://doi.org/10.1029/2018JB016757>
- Szabo, Z., & Zapecza, O. S. (1993). Geologic and geochemical factors controlling uranium, radium-226, and radon-222 in ground water, Newark Basin, New Jersey. In L. C. S. Gundersen, & R. B. Wanty (Eds.), *Field studies of radon in rocks, soils, and water*, (pp. 243–266). Boca Raton, Florida, USA: C.K. Smoley, CRC Press.
- Tissot, B. P., & Welte, D. H. (1984). *Petroleum formation and occurrence*. (Second Revised and Enlarged ed.). Berlin Heidelberg GmbH: Springer-Verlag. <https://doi.org/10.1007/978-3-642-87813-8>
- Tung, S., & Masterlark, T. (2018). Resolving source geometry of the 24 August 2016 Amatrice, central Italy, earthquake from InSAR data and 3D finite-element modeling. *Bulletin of the Seismological Society of America*, 108(2), 553–572. <https://doi.org/10.1785/0120170139>
- Wakita, H., Nakamura, Y., & Sano, Y. (1988). Short-term and intermediate-term geochemical precursors. *Pure and Applied Geophysics*, 126(2–4), 267–278. <https://doi.org/10.1007/BF00878999>
- Wang, C., Elsworth, D., Fang, Y., Liu, K., & Jia, Y. (2017). Weakening effects of microstructural tribological films in CO₂-altered reservoirs and caprocks. In A. R. M. Association (Ed.), 25–28 June, *51st US Rock Mechanics/Geomechanics Symposium* (pp. 1047–1054). San Francisco, California, USA.
- Wang, C., & Manga, M. (2010). *Earthquakes and water*. Berlin Heidelberg: Springer-Verlag.
- Wästeby, N., Skelton, A., Tollefsen, E., Andrén, M., Stockmann, G., Claesson Liljedahl, L., et al. (2014). Hydrochemical monitoring, petrological observation, and geochemical modeling of fault healing after an earthquake. *Journal of Geophysical Research: Solid Earth*, 119, 5727–5740. <https://doi.org/10.1002/2013JB010715>
- Weinlich, F. H. (2014). Carbon dioxide controlled earthquake distribution pattern in the NW Bohemian swarm earthquake region, western Eger Rift, Czech Republic—Gas migration in the crystalline basement. *Geofluids*, 14(2), 143–159. <https://doi.org/10.1111/gfl.12058>
- Wieser, M., and D. Tutas (2009). High precision boron isotope analyses—Negative thermal ionization analysis and static multicollection, *Application Note: 30022 Rep.*, Thermo Scientific, <https://assets.thermofisher.com/TFS-Assets/CMD/Application-Notes/AN-30022-TIMS-Boron-Isotope-AN30022-EN.pdf>.
- Wright, M. T., Stollenwerk, K. G., & Belitz, K. (2014). Assessing the solubility controls on vanadium in groundwater, northeastern San Joaquin Valley, CA. *Applied Geochemistry*, 48, 41–52. <https://doi.org/10.1016/j.apgeochem.2014.06.025>
- Zeng, X., Lin, Y., Chen, W., Bai, Z., Liu, J. Y., & Chen, C. H. (2015). Multiple seismo-anomalies associated with the M6.1 Ludian earthquake on August 3, 2014. *Journal of Asian Earth Sciences*, 114, 352–361. <https://doi.org/10.1016/j.jseaes.2015.04.027>
- Zhu, C., & Anderson, G. (2002). *Environmental applications of geochemical modeling*. Cambridge: Cambridge University Press.